

Supporting Information

Design of the enzymatic biofuel cell with large power output

Yun Chen,^{‡a} Panpan Gai,^{‡a} Jianrong Zhang,^{*a,b} and Jun-Jie Zhu^{*a}

^a State Key Laboratory of Analytical Chemistry for Life Science, School of Chemistry and Chemical Engineering, Nanjing University, Nanjing, 210093, P. R. China.

^b School of Chemistry and Life Science, Nanjing University Jinling college, Nanjing 210089, P. R. China.

Contents:

- (1) The morphology of graphene and graphene–gold nanoparticles (AuNPs) hybrid
 - (2) Cyclic voltammograms (CVs) of the AuNPs, AuNPs–glucose oxidase (GOD), graphene, and graphene–GOD modified electrodes for the absence and presence of glucose
 - (3) CVs of the GOD modified electrode at different scan rates
 - (4) The relationship of the concentrations of GOD and the reduction peak currents of bioanodes
 - (5) CVs of glass carbon electrode and graphene–AuNPs hybrid electrode for HABTS⁻
 - (6) UV-visible spectra for the oxidation of HABTS⁻ by laccase
 - (7) The relationship of the O₂ reduction and the concentration of ABTS
 - (8) The relationship of the power output and the concentration of glucose
 - (9) Blanks and controls experimental results for the maximal power output (P_{max}) of the enzymatic biofuel cell (EBFC)
 - (10) The relationship of P_{max} and storage time
 - (11) The potential value of the EBFC as the power source
-
- (1) The morphology of graphene and graphene–AuNPs hybrid

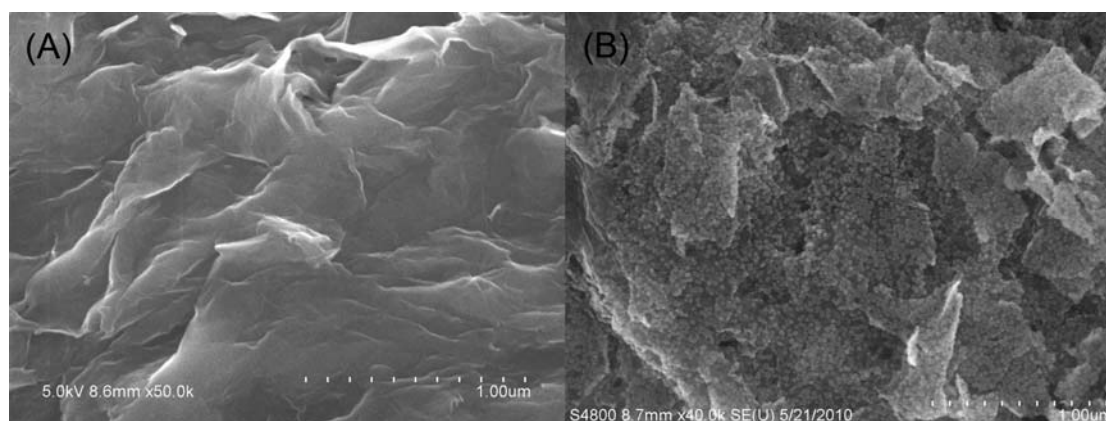


Fig. S1. FESEM image of (A) graphene and (B) graphene–AuNPs hybrid.

The hydrophilic and carboxyl group functionalized graphene–AuNPs hybrid was synthesized *in situ* which was reported by our group previously.¹ The morphology of the hybrid was studied by FESEM. Compared to Fig. S1A, Fig. S1B showed that homogenous AuNPs were attached to the graphene surface and scattered well on the nanosheets. It is known that graphene conducts electricity faster at room temperature than anything else,² and the AuNPs could provide a suitable microenvironment for enzymes immobilization, and facilitate electron transfer between the immobilized enzymes and electrode substrate. Therefore, the graphene–AuNPs hybrid could

realize the direct electron transfer between the catalytic centre of enzymes and electrodes. In addition, as the homogenous dispersive AuNPs on the graphene, the effective loading amount of enzymes was improved.

(2) CVs of the AuNPs, AuNPs–GOD, graphene, and graphene–GOD modified electrodes for the absence and presence of glucose

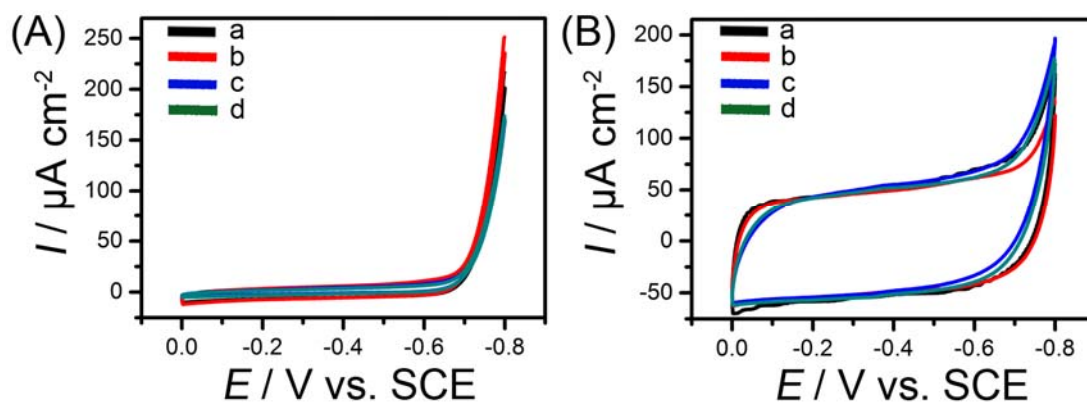


Fig. S2. (A) CVs of the AuNPs electrode in pH 5.0 electrolyte solution saturated with N_2 , (a) without glucose and (c) with 1 mM glucose, and the AuNPs–GOD electrode in the above mentioned solution, (b) without glucose and (d) with 1 mM glucose; (B) CVs of the graphene electrode in pH 5.0 electrolyte solution saturated with N_2 , (a) without glucose and (c) with 1 mM glucose, and the graphene–GOD hybrid in the above mentioned solution, (b) without glucose and (d) with 1 mM glucose. The scan rate was 10 mV s^{-1} .

CVs results showed that for the graphene electrode, AuNPs electrode, and AuNPs–GOD electrode, when glucose was added into the testing solution, there was nearly no change comparing to the CVs results of these electrodes in the same solution without glucose, respectively; while for the graphene–GOD electrode, after the addition of glucose, CV result showed the slight increase of the oxidation current and the decrease of the reduction current, which demonstrated that the GOD on the graphene electrode only performed the weak catalytic role for the oxidation of glucose.

(3) CVs of the GOD modified electrode at different scan rates

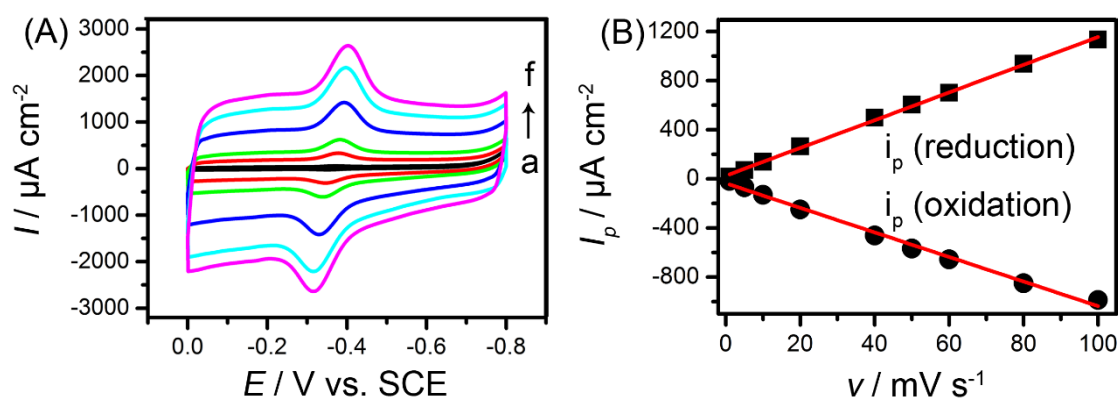


Fig. S3. (A) CVs of the graphene–AuNPs–GOD hybrid electrode at different scan rates: (a) 1

mV s⁻¹, (b) 10 mV s⁻¹, (c) 20 mV s⁻¹, (d) 50 mV s⁻¹, (e) 80 mV s⁻¹ and (f) 100 mV s⁻¹. (B) Plot of redox peak currents *versus* various scan rates from 1 mV s⁻¹ to 100 mV s⁻¹.

CVs of the graphene–AuNPs–GOD hybrid electrode at different scan rates were studied. As shown in Fig. S3A, the formal potential ($E_{GOD}^{o'}$) was independent of the scan rate ranging from 1 to 100 mV s⁻¹. The ratios of the oxidation peak currents to the reduction peak currents at different scan rates were close to 1. The average electron transfer number at different scan rates was estimated to be 2. Furthermore, Fig. S3B showed a characteristic linear proportionality between the peak currents and scan rates. These results indicated that the redox process of GOD was a reversible and surface-confined process.³

(4) The relationship of the concentrations of GOD and the reduction peak currents of bioanodes

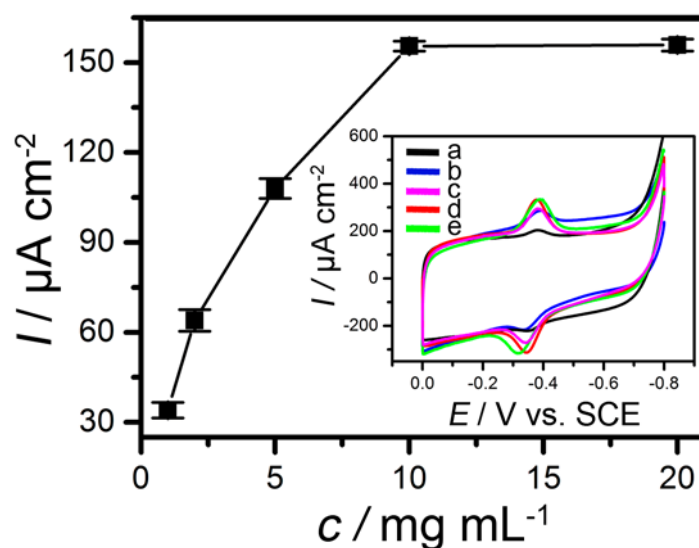


Fig. S4. The relationship between the reduction peak currents of the bound GOD and the concentration of the GOD in pH 5.0 buffer solution at the substrate electrode covered by 240 $\mu\text{g cm}^{-2}$ of the graphene–AuNPs hybrid. Every point was an average value of three independent measurements. Inset: CVs of graphene–AuNPs–GOD hybrid electrodes modified by various concentrations of the GOD: (a) 1 mg mL⁻¹, (b) 2 mg mL⁻¹, (c) 5 mg mL⁻¹, (d) 10 mg mL⁻¹, and (e) 20 mg mL⁻¹. The scan rate was 10 mV s⁻¹, and the pH 5.0 electrolyte solution was saturated with N₂.

To obtain the optimal GOD concentration for the fabrication of bioanode, the reduction peak currents of bioanodes which were immersed into different concentrations of GOD were investigated by cyclic voltammetric measurements in 0.2 M pH 5.0 acetic acid buffer solution, and the results were shown in Fig. S4. With an increase of the concentration of the GOD from 1 mg mL⁻¹ to 10 mg mL⁻¹, the reduction peak currents of GOD increased obviously. However, the reduction peak currents kept stable while the concentration of the GOD was more than 10 mg mL⁻¹. Thus, 10 mg mL⁻¹ was selected as the optimal concentration of GOD for the fabrication of bioanode.

(5) CVs of glass carbon electrode and graphene–AuNPs hybrid electrode for HABTS⁻

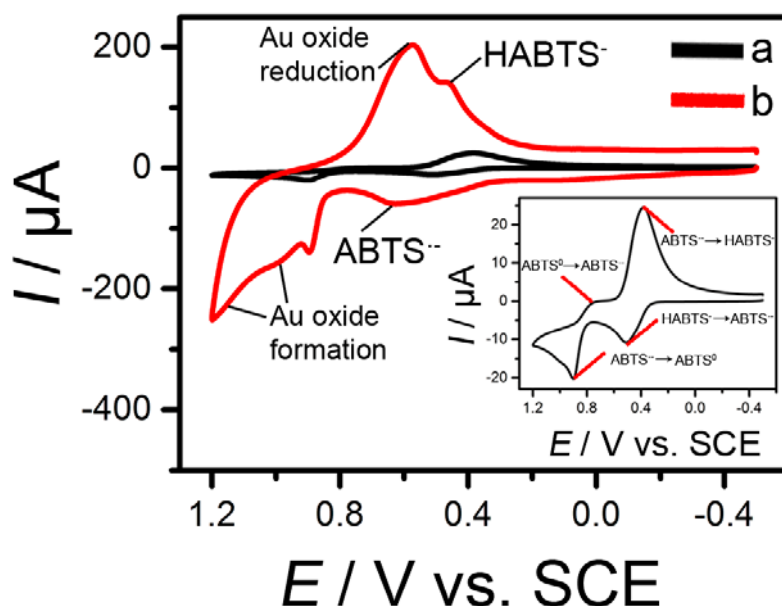


Fig. S5. CVs of (a) glass carbon electrode and (b) graphene–AuNPs hybrid electrode in 0.2 M acetic acid buffer solution (pH 5.0) containing 0.5 mM ABTS saturated with N₂. Inset: the enlargement of curve a.

It is reported that in 1.5 M HClO₄ testing solution, ABTS²⁻ should be changed to HABTS⁻, and the CV results showed two characteristic reversible one-electron waves at glass carbon electrode, while under the same CV testing conditions, ABTS²⁻ showed two anodic waves but only one cathodic wave in near neutral testing solution.⁴ Our results unambiguously showed that two waves appeared and it demonstrated that HABTS⁻ existed in the testing solution. In addition, because the adsorption of the acid media was superior at the surface of graphene–AuNPs hybrid,⁵ more HABTS⁻ should form at the surface of the electrode, then, the redox potential of ABTS²⁻/HABTS⁻ couple increased to around 0.55 V (vs. SCE), which is very similar to the reported result.⁶

(6) UV-visible spectra for the oxidation of HABTS⁻ by laccase

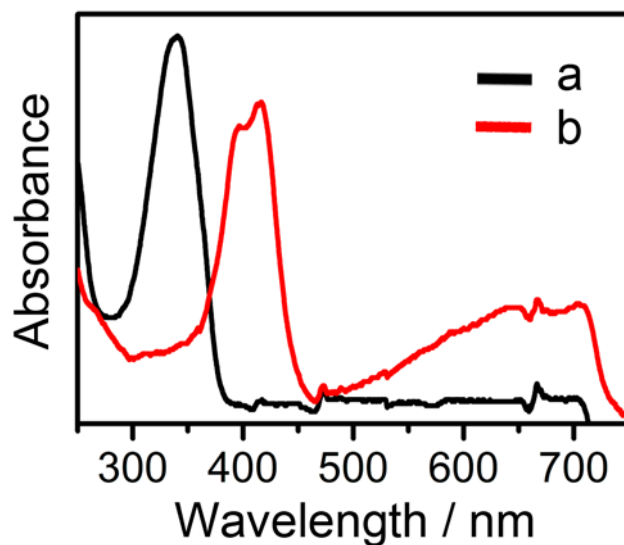


Fig. S6. UV-visible spectra of (a) HABTS^- and (b) HABTS^- oxidized by laccase.

UV-visible spectra showed that the HABTS^- could be oxidised by laccase, and the product $\text{ABTS}^{\bullet-}$ showed the three peak at 417, 645, and 709 nm.⁴

(7) The relationship of the O_2 reduction and the concentration of ABTS

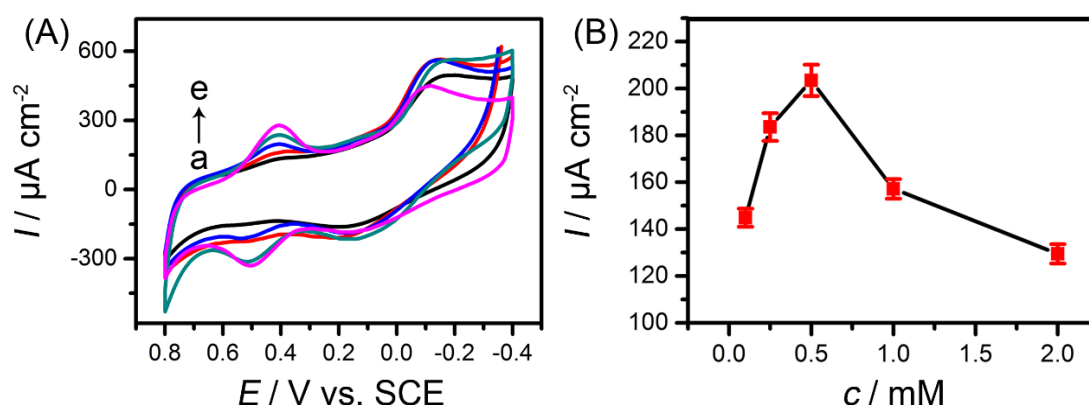


Fig. S7. (A) CVs of the graphene-AuNPs-laccase hybrid electrode in 0.2 M acetic acid buffer solution (pH 5.0, the concentrations of ABTS were as follows, (a) 0.1 mM, (b) 0.25 mM, (c) 0.5 mM, (d) 1 mM and (e) 2 mM) saturated with O_2 at the scan rate of 10 mV s^{-1} . (B) The relationship of the reduction peak current of saturated O_2 and the concentrations of ABTS. Every point was an average value of three independent measurements.

To obtain the optimal catalytic current of saturated O_2 , the reduction peak current of saturated O_2 in 0.2 M acetic acid buffer solution with the different concentrations of ABTS was investigated by cyclic voltammetric measurements as shown in Fig. S7A. Fig. S7B showed the relationship between the concentrations of ABTS and the reduction peak current of saturated O_2 . With an increase of the concentration of the ABTS from 0.1 mM to 0.5 mM, the reduction peak currents of saturated O_2 enhanced obviously. However, the reduction peak currents decreased while the concentration of the ABTS was more than 0.5 mM. Therefore, 0.5 mM was selected as the optimal

concentration of ABTS for the reduction of saturated O_2 at the graphene–AuNPs–laccase hybrid electrode.

(8) The relationship of the power output and the concentration of glucose

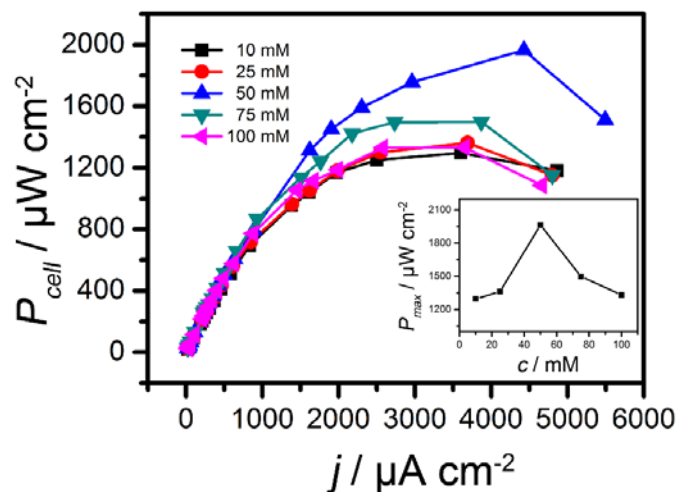


Fig. S8. Power density curves of the enzymatic biofuel cell, the bioanode compartment contained various glucose concentrations from 10 mM to 100 mM. Inset: the relationship of the P_{max} of the enzymatic biofuel cell and the glucose concentrations.

The power density of the enzymatic biofuel cell is dependent on the glucose concentration.⁷ In order to investigate the relationship of the P_{max} of the enzymatic biofuel cell and the glucose concentrations, a series of glucose concentrations in the bioanode compartment was studied. After the concentration of the glucose changed from 10 mM to 50 mM, the P_{max} enhanced up to $1.96 \pm 0.13 \text{ mW cm}^{-2}$. However, when the concentration of the glucose was more than 50 mM, the P_{max} decreased obviously. Therefore, 50 mM could be used as the optimal concentration of glucose for the P_{max} of the enzymatic biofuel cell.

(9) Blanks and controls experimental results for the P_{max} of the EBFC

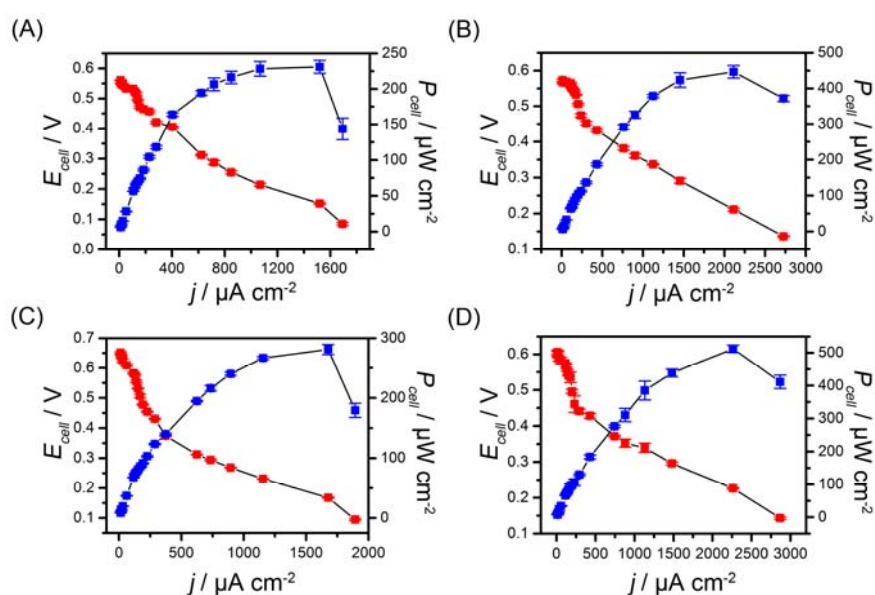


Fig. S9. Polarization curve and power density curve of the enzymatic biofuel cell under the optimal conditions, (A) without glucose and (B) without GOD in the bioanode; (C) without O₂ and (D) without laccase in the biocathode. Every point was an average value of three independent measurements.

Under the optimal conditions and in the absence of glucose or O₂, the blank experimental results showed that the maximal power output of the enzymatic biofuel cell was only $0.231 \pm 0.009 \text{ mW cm}^{-2}$ or $0.281 \pm 0.008 \text{ mW cm}^{-2}$, respectively; In the absence of glucose oxidase in bioanode or laccase in biocathode, the control experimental results displayed that the maximal power output of the enzymatic biofuel cell was only $0.447 \pm 0.018 \text{ mW cm}^{-2}$ or $0.512 \pm 0.011 \text{ mW cm}^{-2}$, respectively, which demonstrated that the response was due only to glucose oxidation catalyzed by glucose oxidase and oxygen reduction catalyzed by laccase.

(10) The relationship of P_{max} and storage time

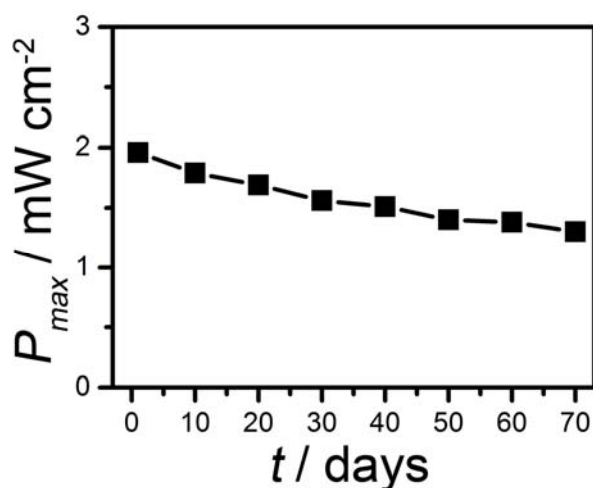


Fig. S10. The relationship of the P_{max} of the EBFC and the storage time.

Under the optimal conditions, the P_{max} of the fresh prepared EBFC was as high as 1.96 mW cm^{-2} . For evaluating the stability of the EBFC, the P_{max} of EBFC was tested every day. After the operation of about 70 days, the P_{max} of EBFC decreased to about 1.30 mW cm^{-2} , about 66% of its optimal value.

(11) The potential value of the EBFC as the power source

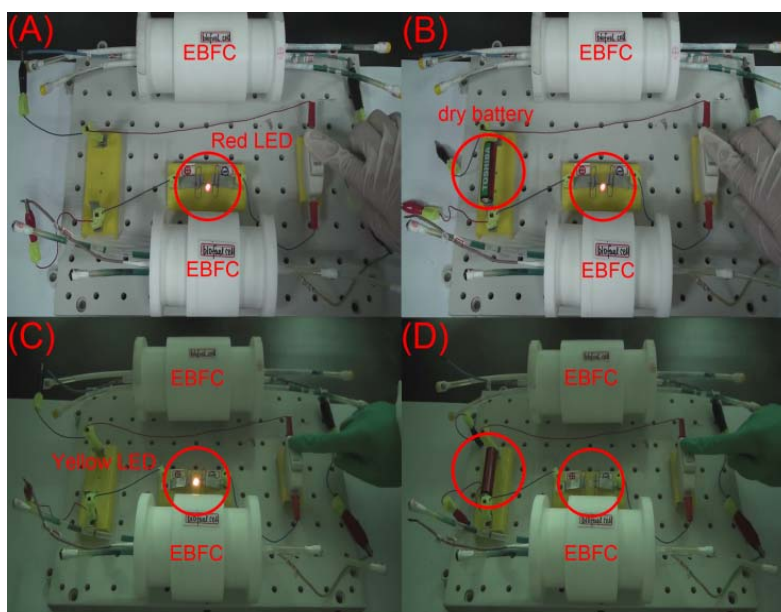


Fig. S11. The cell unit of the two as-prepared EBFC units in series as the power source for (A) the red LED and (C) the yellow LED, respectively. A dry battery as the power source for (B) the red LED and (D) the yellow LED, respectively.

The standard operating voltages of the red and yellow LED are 1.6 V⁸ and 1.8 V, respectively. Thus, both the designed EBFC in series can match the operating voltage of the LEDs. Fig. S11A displayed that the red LED was lighted obviously once the circuit was powered by both the as-prepared EBFC in series. The light intensity was nearly the same as that of a dry battery (TOSHIBA, $E_{cell}^{ocv} = 1.62$ V) as shown in Fig. S11B. Fig. S11C displayed that both the EBFC models in series could also light the yellow LED. However, it was noted that only a feeble light could be observed when the yellow LED was powered by a dry battery, as shown in Fig. S11D. The reason was that the operating voltage of a yellow LED was higher than that of a dry battery.

References

- 1 Y. Chen, Y. Li, D. Sun, D. Tian, J. Zhang and J.-J. Zhu, *J. Mater. Chem.*, 2011, **21**, 7604.
- 2 R. F. Service, *Science*, 2008, **322**, 1785.
- 3 C. S. Shan, H. F. Yang, J. F. Song, D. X. Han, A. Ivaska and L. Niu, *Anal. Chem.*, 2009, **81**, 2378.
- 4 S. L. Scott, W. Chen, A. Bakac, and J. H. Espenson, *J. Phys. Chem.*, 1993, **97**, 6710.
- 5 Y. Önal, S. Schimpf, and P. Claus, *J. Catal.*, 2004, **223**, 122.
- 6 S. C. Barton, J. Gallaway and P. Atanassov, *Chem. Rev.*, 2004, **104**, 4867.
- 7 D. Wen, X. L. Xu and S. J. Dong, *Energy Environ Sci.*, 2011, **4**, 1358.
- 8 T. Miyake, S. Yoshino, T. Yamada, K. Hata and M. Nishizawa, *J. Am. Chem. Soc.*, 2011, **133**, 5129.